Geophys. J. Int. (2000) **141,** 479–484

Slab pull effects from a flexural analysis of the Tonga and Kermadec trenches (Pacific Plate)

Daniel Garcia-Castellanos,* Montserrat Torne and Manel Fernàndez
Department of Geophysics, Institute of Earth Sciences 'Jaume Almera', CSIC, Solé i Sabarís s/n, 08028 *Barcelona, Spain*

Accepted 1999 December 9. Received 1999 November 23; in original form 1999 March 1

SUMMARY

Thin-plate flexure models have been frequently used to explain the mechanical behaviour of the lithosphere at oceanic trenches, but little attention has been paid to using them as a way to check the relative importance of different plate-driving mechanisms. A 2-D numerical algorithm accounting for the flexural deflection of the lithosphere controlled by multilayered elastic–plastic rheology (brittle–elastic–ductile) has been applied to the seaward side of the Tonga and Kermadec trenches. This approach gives a better fit to the bathymetry on both trenches than assuming classical homogeneous plate models, and allows the interplate coupling forces and the lithospheric strength profile to be constrained. Our results show that, in order to fit the observed deflection of the lithosphere, a regional tensile horizontal force must act in both regions. This tensile force and its flexural effects are discussed in terms of slab pull as a main plate-driving mechanism. The predicted stress and yielding distributions partially match the outer-rise earthquake hypocentres within the subducting plate, and thus do not invalidate the model.

Key words: flexure, oceanic lithosphere, rheology, slab pull.

INTRODUCTION

Various observable features in the ocean, such as deep-sea trenches and their ocean-side outer rises, have been interpreted in terms of flexure of the subducting oceanic lithosphere, considering either an elastic (Caldwell *et al.* 1976), viscous (De Bremaecker 1977), viscoelastic (Melosh 1978), perfectly plastic (Lobkovsky & Sorokhtin 1976), or elastic–plastic behaviour (McAdoo *et al.* 1978). Although these homogeneous plate models can reproduce the main flexural features, they fail to account for a reasonable stress distribution within the lithosphere. This is in contradiction to the concept of a yield stress envelope (Goetze & Evans 1979), which predicts minimum strength at the top and the bottom of the mechanical lithosphere. Bodine *et al.* (1981) quantitatively linked flexure with the yield stress envelope (YSE), avoiding the need to impose an arbitrary value for the thickness of the plate and proposing a moment-curvature formulation that allows the flexure to be calculated with more realistic stress distributions.

This detailed lithosphere rheology, which can substantially modify the force balance obtained by modelling flexure, has been frequently ignored in oceanic flexural studies, and therefore little attention has been paid to the information about the plate driving mechanisms that flexure can provide. In the last two decades it has been generally accepted (e.g. Jurdy & Stefanick 1991) that plate tectonics is driven mainly by the plate boundary forces, such as slab pull, which may be detectable through flexural modelling.

In this study we use an algorithm (Garcia-Castellanos *et al.* 1997) based on an approach similar to that of Bodine *et al.* (1981) and Waschbusch & Royden (1992) to constrain the forces operating in the trench axis, the bending stress distribution and the thermal structure of the subducting lithosphere seawards of the Tonga and Kermadec trenches. These trenches are the topographic consequence of the subduction of the Pacific oceanic plate (105 Ma) under the Indo-Australian Plate (Fig. 1). The Pacific Plate subducts at a rapid rate of 5.5–7.4 cm yr^{-1} (Jarrard 1986), generating most of the world's deep earthquakes and producing a deep slab that penetrates the lower mantle (van der Hilst 1995). The absence of a remarkable forebulge, together with the large slab length and the age of the Pacific Plate in the region, suggests that the tensional force related to slab pull may be large in this area. Thereby, the main objective of this work is to find evidence of the slab pull force using a flexural model that is consistent with the thermal and rheological structure of the lithosphere.

* Now at: Tectonic/Structural Geology Group, Vrije Universiteit, De Boelelaan 1085, 1081 HV, Amsterdam, the Netherlands. E-mail: gard@geo.vu.nl

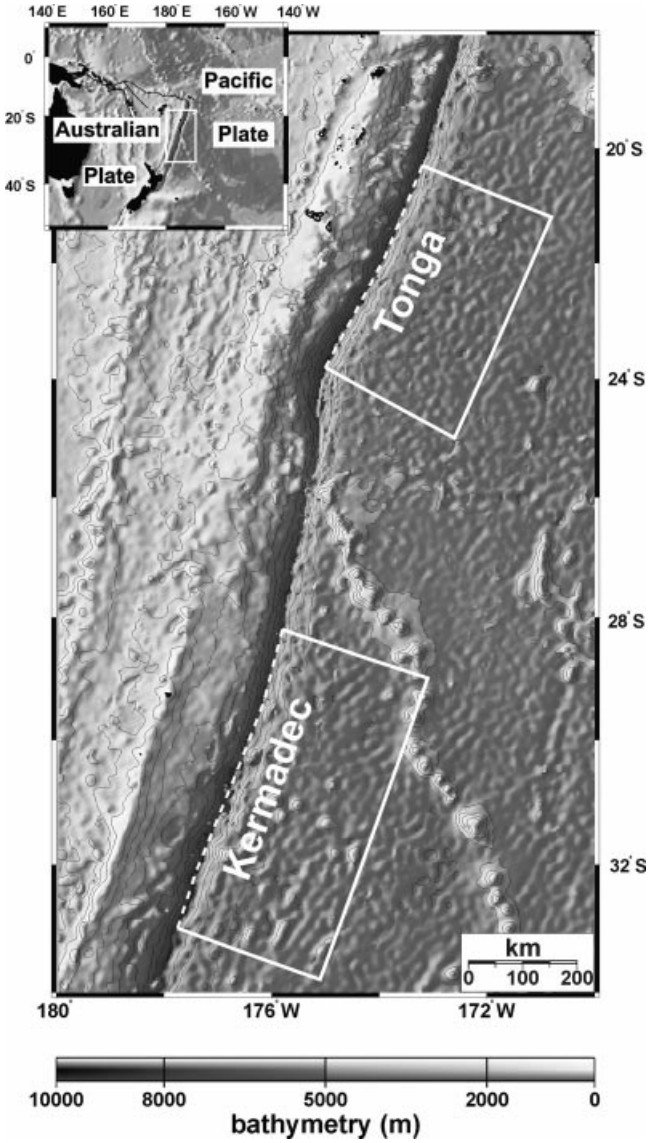

Figure 1. Location map of the study region. The rectangles show the model Tonga and Kermadec regions (dashed lines show the trench axis). The left upper inset shows a global view of the area. The seafloor depth in the Pacific Plate increases from about 5700 m in the non-flexed region to more than 9500 m in some parts of the trench axis. The bathymetric contour interval 1000 m.

METHODOLOGY

We have developed a 2-D finite difference algorithm (Garcia-Castellanos *et al.* 1997) that accounts for the YSE depth-dependent rheology to calculate the deflection of the lithosphere in response to applied in-plane (vertical and horizontal) tectonic forces (Fig. 2). The YSE is used to limit the stresses produced during the bending of the plate, which is accomplished following the moment-curvature iteration described by McNutt (1984) and Waschbusch & Royden (1992). Limiting bending stresses leads to important lateral changes of the equivalent elastic thickness (T_e) and strongly modifies the deflection pattern. This heterogeneous plate model also differs from the homogeneous ones (elastic, viscous, viscoelastic) in that T_e is calculated from the assumed thermal regime and the rheological parameters.

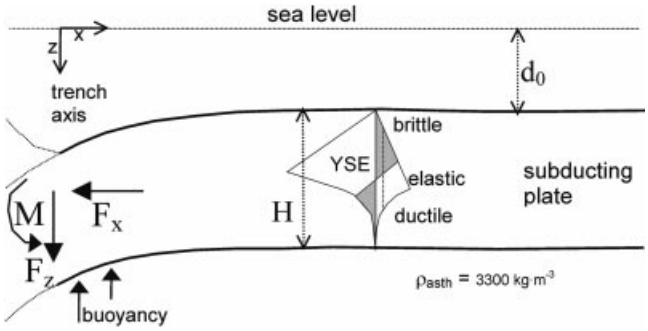

Figure 2. Cartoon showing the forces acting on a subducting plate. Bending is caused by an applied moment M, vertical force F_z and horizontal force F_x acting at the trench axis (the arrows show the positive sense). Far enough from the trench, the plate preserves its reference depth d_0. The mechanical response of the plate is controlled by the yield stress envelope (Fig. 3) and the mechanical thickness H of the lithosphere (the depth at which the strength is less than 10 MPa).

Fig. 3 shows the results obtained with two different YSEs based on the temperature distribution at depth obtained by the cooling plate models of Parsons & Sclater (1977) and Stein & Stein (1992), referred to hereafter as P & S and S & S. Both

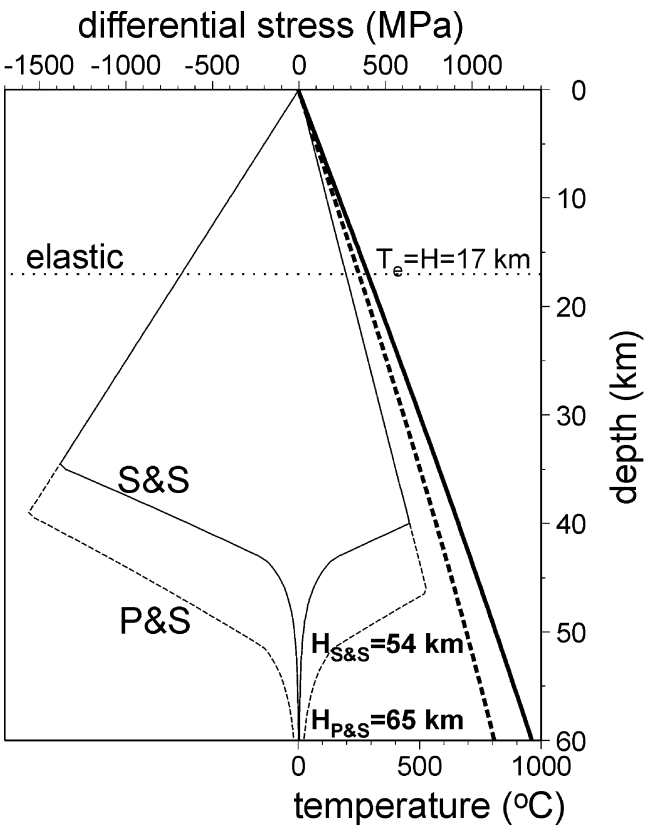

Figure 3. Yield stress envelope (YSE) of a 105 Ma lithosphere assuming a strain rate of 10^{-16} s^{-1} and the temperature structure from the cooling plate model of Parsons & Sclater (1977) (dashed line) and Stein & Stein (1992) (thin line). The best-fitting elastic plate in our modelling requires an elastic thickness $T_e = 17$ km. The bold lines are the corresponding geotherms.

models relate the temperature distribution to the age of the oceanic lithosphere assuming that this lithosphere behaves as a cooling plate after spreading from the mid-oceanic ridge. The main differences between the models are the different surface heat flow data sets that are used, and consequently the different best-fit parameters that are obtained. As a result, the S & S model predicts a hotter thermal regime than the P & S model does.

Our modelling domain covers the area of the plate that is still not subducted; that is, seawards of the trench axis (Fig. 1). In this domain, the bathymetry is fitted by varying the boundary conditions at the subducting edge of the plate model (trench axis, $x = 0$). These boundary conditions consist of a force (F_x, F_z) and a moment (M) which, together with the asthenospheric buoyancy, are the only external forces acting on the plate (Fig. 2). Assuming the thin plate approach (e.g. Turcotte & Schubert 1982), any load distribution landwards of the trench axis can be represented by these three forces. Other possible intraplate forces, such as mantle shear force acting at the base of the lithosphere, are ignored.

The best fit (the minimum mean difference between observed bathymetry and that predicted by the model) is found by iteratively varying the vertical force and the moment for various reasonable values of the horizontal force. About 10^4 combinations of these parameters have been tested to find the best-fitting set for each plate model. This has been undertaken semi-automatically by initially defining a domain in the parameter field in which 16 parameter sets are tested. Then, the domain is successively reduced to the vicinity of the best-fitting area, where 16 new parameter sets are tested.

DATA

Rather than taking a particular bathymetric transect across the Tonga and Kermadec trenches, we have computed, for each study area, an average bathymetric profile that is representative of a wider region of the plate seawards of both trenches (Fig. 1). To obtain the averaged bathymetric profiles shown in Fig. 4, one data point was calculated every 4 km by projecting bathymetric values within a 430-km wide strip onto the profile for the Tonga trench and within a 560-km wide strip for the Kermadec trench. Standard deviations were calculated to estimate the importance of lateral variations along the strike and of the high-frequency variations. The bathymetry of both regions has been taken from direct altimetric measures contained in the world database of Smith & Sandwell (1997). We applied no corrections for variations of sediment thickness owing to the thin sedimentary cover of the region and its homogeneous distribution. Furthermore, we have not applied any corrections for tilting due to lithospheric cooling (Parsons & Sclater 1977) owing to the small variations of the age of the seafloor in the study regions.

The parameter values used for the thermal plate models are the mean values used by Stein & Stein (1992) (plate thickness $a = 95$ km; basal temperature $T_m = 1450\,^{\circ}\mathrm{C}$) and by Parsons & Sclater (1977) ($a = 125$ km; $T_m = 1350\,^{\circ}\mathrm{C}$). Two geotherms have been constructed, according to these models, using an age for the oceanic lithosphere of 105 ± 10 Ma (Jarrard 1986). These geotherms define two YSEs assuming the rheological parameters given by Goetze & Evans (1979) (Fig. 3).

To assess the model stress distribution independently, we use the earthquake hypocentre distribution and the associated focal mechanisms in the Tonga region. These data have been taken from the 1990 USGS/NEIC Hypocentre Associated Data Base and the ISC Bulletin Data Base (NEIC 1990). In our compilation, we have only used earthquakes with magnitude greater than 3. Owing to the scarcity of earthquake data we have taken a wider region (1050 km along the trench axis) than that considered to construct the bathymetric profiles.

RESULTS AND DISCUSSION

Fig. 4 shows the profiles for the best-fitting parameters shown in Table 1. In this figure, it can be seen that the multiple-

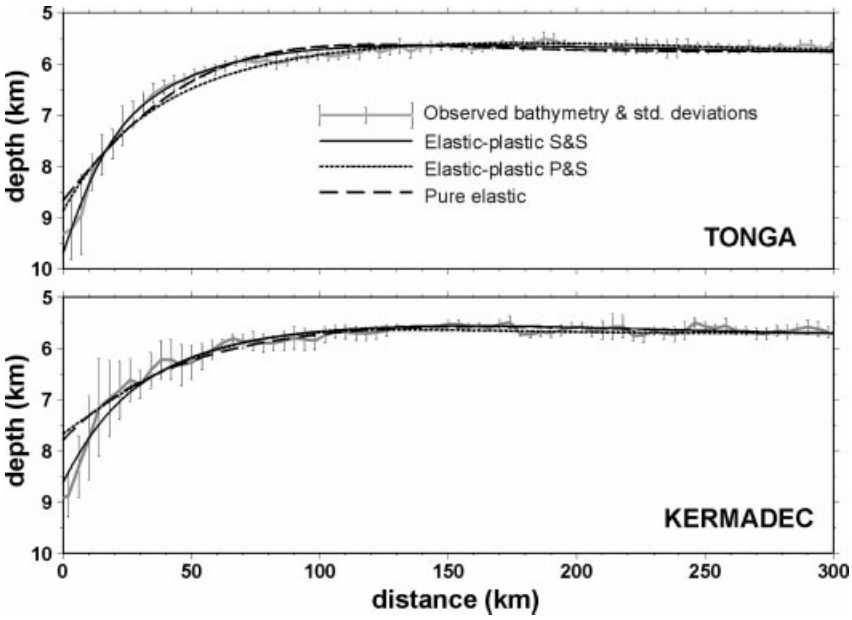

Figure 4. Observed bathymetry (thick grey line) and best-fitting deflection profiles using the elastic plate model ($T_e = 17$ km) and the elastic–plastic models governed by the Stein & Stein (1992) and Parsons & Sclater (1977) plate cooling models (S & S and P & S, respectively).

Table 1. Force and moment values that best fit the bathymetry of the Tonga and Kermadec trenches for various rheologies and cooling plate models.

Plate model	Moment M [10^{16} N] (± 1.0)	Vertical force F_z [10^{12} Nm^{-1}] (± 1.0)	Horizontal force F_x [10^{12} Nm^{-1}] (± 2.0)	Mean error $\langle \Delta\omega \rangle$ [m]
TONGA				
Elastic-plastic S & S	10.5	7.5	4.0	59
Elastic-plastic P & S	13.8	3.0	8.0	83
Pure elastic (Te = 17 km)	1.3	1.7	10.0	108
KERMADEC				
Elastic-plastic S & S	9.9	3.0	4.0	83
Elastic-plastic P & S	10.8	1.2	10.0	91
Pure elastic (Te = 17 km)	−0.1	1.3	10.0	104

S & S and P & S refer to the Stein & Stein (1992) and Parsons & Sclater (1977) cooling plate models, respectively. Te is the effective elastic thickness for a pure elastic model.

layer elastic–plastic profiles are in better agreement with the observed bathymetry than the pure elastic profile, since the observed slope and curvature of the plate are greater than that predicted by the elastic plate model. Similar results were obtained in the Tonga trench by Turcotte *et al.* (1978) using an elastic–perfectly plastic analysis, which differs from our approach in that it uses an unrealistic constant strength within the lithosphere. As seen in Table 1, ignoring the depth dependence of the strength (elastic plate) can induce important errors when calculating the boundary forces. The reference plate depths d_0 are 5750 m for Tonga and 5800 m for Kermadec.

The results also show that the S & S cooling plate model fits the bathymetry better in both trenches than the P & S cooling model does (Fig. 4 and Table 1). This is related to the fact that the P & S model predicts a colder lithosphere which cannot reproduce the observed high plate curvature. However, the uncertainties in the rheological and thermal parameters (Panteleyev & Diament 1993; Parsons & Sclater 1977; Stein & Stein 1992) mean than these results should be interpreted as favouring a certain strength profile, rather than a certain thermal structure or mantle rheology. The strength profile corresponding to the best-fitting model is characterized by a mechanical thickness of $H = 54$ km (defining the mechanical lithosphere as the layer with strength greater than 10 MPa).

In both trenches, the best-fitting model is defined by the applied moment and the vertical and horizontal forces. As observed from Table 1, the resulting moments and horizontal forces are very similar in the two areas ($F_x = 4.0 \times 10^{12}$ N m^{-1} and $M \sim 10^{17}$ N), whilst the vertical force is $F_z = 7.5 \times 10^{12}$ and $F_z = 3.0 \times 10^{12}$ N m^{-1} in the Tonga and Kermadec trenches, respectively. The magnitudes of the vertical forces acting in the Tonga and Kermadec trenches are in the same range as those computed by Royden (1993) for the Apennines and Hellenides subduction boundaries.

The most outstanding result is that the best-fitting model for both trenches is obtained when applying a tensile force of $F_x = 4.0 \pm 2 \times 10^{12}$ N m^{-1}. As illustrated in Fig. 5(a), such a tensile force yields the minimum mean difference between the observed and calculated bathymetry when an elastic–plastic rheology and the S & S cooling plate model are assumed. However, even when the thermal regime and rheological behaviour are varied, a tensile horizontal force is still needed to minimize the deflection misfit. This tensile horizontal force permits us to increase the deflection of the plate and simultaneously reduce the amplitude of the outer rise (forebulge) at the expense of varying the vertical force and the applied moment (Fig. 5b). In order to illustrate how horizontal forces affect lithospheric deflection (see Karner *et al.* 1993 for a complete discussion), we have computed the resulting deflection for various values of F_x in the Tonga trench (Figs 5b and c). A decrease in the applied horizontal force from tensile (positive sign) to compressive (negative sign) results in a shallower bathymetry and a noticeable reduction in the plate curvature. Therefore, a null horizontal force results in a bathymetric misfit of about 700 m in the axis of the trench, whereas a compressive force of $F_x = -4.0 \times 10^{12}$ N m^{-1} yields a deflection misfit of more than 1.8 km. In spite of the uncertainty in determining the acting forces ($\pm 1 \times 10^{12}$ N m^{-1} for F_z and M, and $\pm 2 \times 10^{12}$ N m^{-1} for F_x), the observed differences in deflection due to compression and tension allow us to favour the existence of a horizontal tensile force acting across both trenches.

The tensile sign of this force is opposite to that obtained by Liu & McNally (1993). A possible cause of this discrepancy is that they used a purely elastic plate model, which, as mentioned above, is inadequate for predicting realistic stress distributions within the bending lithosphere. In addition, their analysis is mainly based on inversion of earthquake data, which may result in large uncertainties due to the scarcity of events and the errors associated with the location determinations. The tensile sign of the horizontal force favours the slab pull plate-motion mechanism over the ridge push and mantle drag mechanisms, since these would produce a compressive regime near the collision between the two plates. Simple calculations of the slab pull and ridge push forces (e.g. Turcotte & Schubert 1982) give values of $F_{sp} \approx 20 \times 10^{12}$ N m^{-1} and $F_{rp} \approx 3 \times 10^{12}$ N m^{-1}, respectively. Following Liu & McNally (1993), the resistance that the mantle offers to the subduction of the slab must be of the order of $F_{sh} \approx 1 \times 10^{12}$ N m^{-1}. Assuming dynamical equilibrium in the subduction, we can write the force balance of the subducting plate as

$$F_{sp} - F_{tc} - F_{sh} + F_{rp} - F_{md} = 0,$$

where F_{tc} is the tectonic coupling force between the Australian and Pacific plates and F_{md} is the mantle drag force acting between the trench and the ridge (positive if opposite to the movement of the plate). The forces at each side of the trench

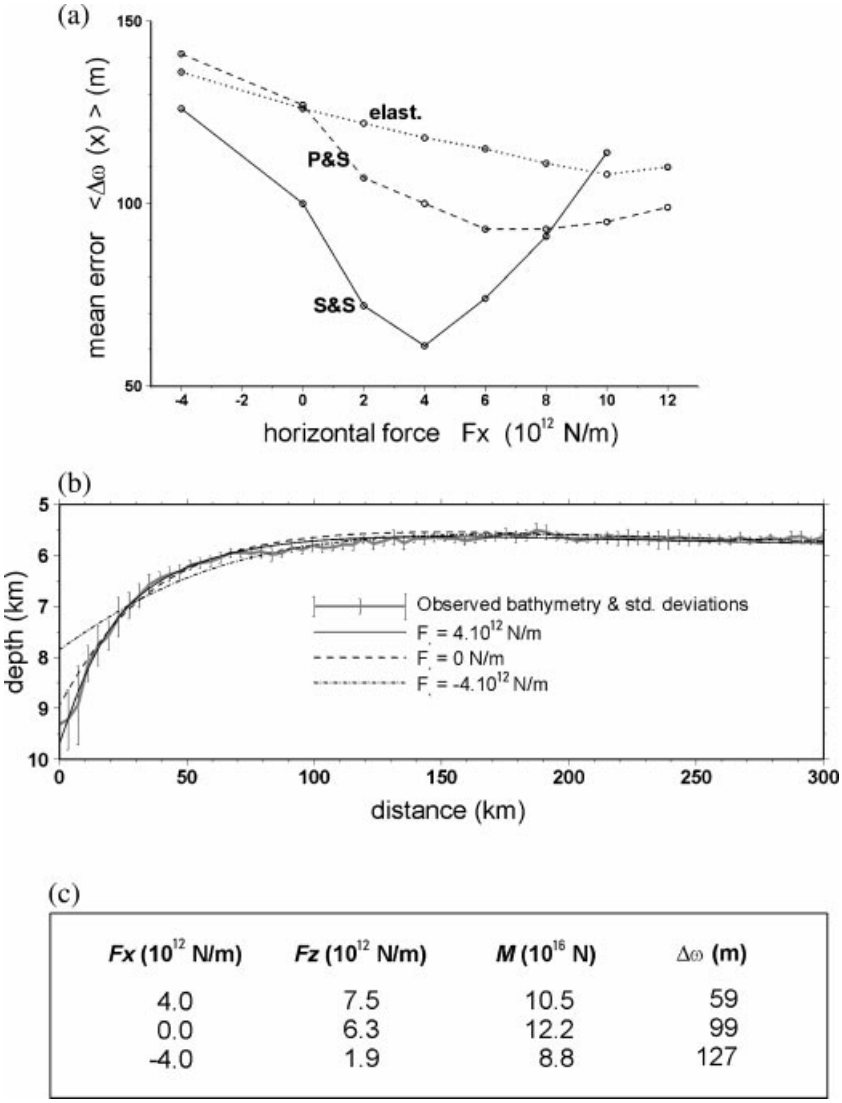

(c)

Fx (10^{12} N/m)	*Fz* (10^{12} N/m)	*M* (10^{16} N)	Δω (m)
4.0	7.5	10.5	59
0.0	6.3	12.2	99
-4.0	1.9	8.8	127

Figure 5. Parametric calculations in the Tonga trench. (a) Mean difference $\langle \Delta\omega \rangle$ between the observed and predicted bathymetry as a function of the applied horizontal force (F_x) for various rheologies (see caption to Fig. 4). (b) Resulting basement deflection from various horizontal forces for the S & S elastic–plastic model (see caption to Fig. 4). (c) Resulting moment (M), vertical force (F_z), and mean deflection misfit ($\Delta\omega$) for the best-fitting models after varying the applied horizontal force (F_x). F_x is positive if tensile.

must be equal to our calculated extensional force F_x:

$$F_x = F_{sp} - F_{tc} - F_{sh},$$

$$F_x = F_{md} - F_{rp}.$$

Assuming this force balance, our resulting tensional force ($F_x > 0$) implies that:

(1) the slab pull force is greater than the tectonic coupling and the resistance to penetrating the mantle;

(2) the mantle drag is a resistance force (i.e. opposed to the plate movement), which is greater than the ridge push, which means that plate movement is driven by slab pull; and

(3) the tectonic coupling force must be of the order of $F_{tc} \approx 15 \times 10^{12}$ N m^{-1}, close to the value obtained by Liu & McNally (1993).

Fig. 6 shows the stress distribution in the Tonga region for the best set of boundary conditions listed in Table 1. In this figure we have also plotted the hypocentres of seismic events located seawards of the Tonga trench, distinguishing between compressional and tensional earthquakes. As observed, the majority of shocks occur in the predicted yielding zone, with focal mechanisms that are in general agreement with the obtained stress distribution. The tensile events are located within the region where our model predicts tensional yielding, whereas compressive events (most of them located in the northern part of Tonga) are located in both the predicted tensile and compressive regions. This misfit could be related to the fact that in our model we have not considered interplate shear forces, which could be relevant in the northern part of the Tonga trench, where the seismic coupling is higher (Scholz & Campos 1995). We also observe that the aseismic zone between the tensile and compressive regimes is seen to correspond to the location of the neutral surface of our model (at about 40 km depth). These comparisons should, however, be taken with some caution due to the uncertainty

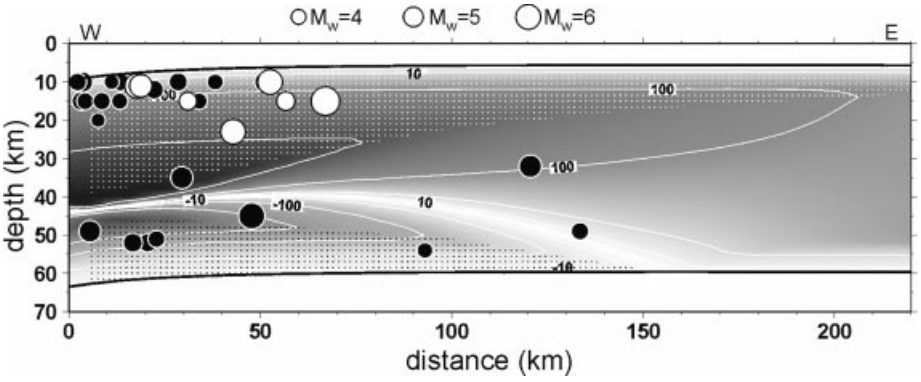

Figure 6. Stress distribution predicted in the Tonga trench (positive when tensional). Circles show the earthquake hypocentre distribution: black circles are compressive shocks and white ones are tensional. The size of the circles is proportional to the earthquake magnitude. Dotted regions correspond to the predicted occurrence of brittle and ductile yielding: black dots for compressive yielding and white for tensional yielding.

of hypocentre locations, which can amount to more than 15 km in depth.

ACKNOWLEDGMENTS

We are deeply indebted to Juan Lorenzo for his interesting comments, which contributed considerably to improving this paper. We are also grateful for the comments and suggestions made on the manuscript version by L. Royden and D. Jurdy. The code we developed in this work is available for public use at ftp://caribe.ija.csic.es/pub/dani/tao/.

REFERENCES

Bodine, J.H., Steckler, M.S. & Watts, A.B., 1981. Observations of flexure and the rheology of the oceanic lithosphere, *J. geophys. Res.,* **86,** 3695–3707.

Caldwell, J.G., Haxby, W.F., Karig, D.E. & Turcotte, D.L., 1976. On the applicability of a universal trench profile, *Earth planet. Sci. Lett.,* **31,** 239–246.

De Bremaecker, J.-C., 1977. Is the oceanic lithosphere elastic or viscous?, *J. geophys. Res.,* **82,** 2001–2004.

Garcia-Castellanos, D., Fernàndez, M. & Torne, M., 1997. Numerical modeling of foreland basin formation: a program relating thrusting, flexure, sediment geometry and lithosphere rheology, *Comput. Geosci.,* **23,** 993–1003.

Goetze, C. & Evans, B., 1979. Stress and temperature in the bending lithosphere as constrained by experimental rock mechanics, *Geophys. J. R. astr. Soc.,* **59,** 463–478.

Jarrard, R.D., 1986. Relations among subduction parameters, *Rev. Geophys.,* **24,** 217–284.

Jurdy, D.M. & Stefanick, M., 1991. The forces driving the plates: constraints from kinematics and stress observations, *Phil. Trans. R. Soc. Lond.,* **337,** 127–139.

Karner, G.D., Driscoll, N.W. & Weissel, J.K., 1993. Response of the lithosphere to in-plane force variations, *Earth planet. Sci. Lett*, **114,** 397–416.

Liu, X. & McNally, K.C., 1993. Quantitative estimates of interplate coupling inferred from outer rise earthquakes, *Pageoph,* **140,** 211–255.

Lobkovsky, L.I. & Sorokhtin, O.G., 1976. Plastic deformation of the lithosphere at a subduction zone, in *Tectonics of Lithospheric Plates,* pp. 22–52, ed. Sorokhtin, O.G., IOAN, Moscow (in Russian).

McAdoo, D.C., Caldwell, J.G. & Turcotte, D.L., 1978. On the elastic-perfectly plastic bending of the lithosphere under generalized loading with application to the Kuril Trench, *Geophys. J. R. astr. Soc.,* **54,** 11–26.

McNutt, M.K., 1984. Lithospheric flexure and thermal anomalies, *J. geophys. Res.,* **89,** 11 180–11 194.

Melosh, H.J., 1978. Dynamic support of the outer rise, *Geophys. Res. Lett.,* **5,** 321–324.

NEIC, 1990. *Source Parameter Data Base,* Hypocenter Associated Data CD-ROM, 1977-March 1989, Version 1.0, NEIC, World Data Center–A, Denver, CO.

Panteleyev, A.N. & Diament, M., 1993. Influence of some rheological parameters on flexure of the oceanic lithosphere, *Geophys. J. Int.,* **114,** 209–220.

Parsons, B. & Sclater, J.G., 1977. An analysis of the variation of ocean floor bathymetry and heat flow with age, *J. geophys. Res.,* **82,** 803–827.

Royden, L., 1993. The tectonic expression of slab pull at continental convergent boundaries, *Tectonics,* **12,** 303–325.

Scholz, C.H. & Campos, J., 1995. On the mechanism of seismic decoupling and back arc spreading at subduction zones, *J. geophys. Res.,* **100,** 22 103–22 115.

Smith, W.H.F. & Sandwell, D.T., 1997. Global seafloor topography from satellite altimetry and ship depth soundings, *Science,* **277,** 1956–1962.

Stein, C.A. & Stein, S., 1992. A model for the global variation in oceanic depth and heat flow with lithospheric age, *Nature,* **359,** 123–129.

Turcotte, D.L. & Schubert, G., 1982. *Geodynamics. Applications of Continuum Physics to Geological Problems,* John Wiley, New York.

Turcotte, D.L., McAdoo, D.C. & Caldwell, J.G., 1978. An elastic-perfectly plastic analysis of the bending of the lithosphere at a trench, *Tectonophysics,* **47,** 193–205.

van der Hilst, R., 1995. Complex morphology of subducted lithosphere in the mantle beneath the Tonga trench, *Nature,* **374,** 154–157.

Waschbusch, P.J. & Royden, L.H., 1992. Spatial and temporal evolution of foredeep basins: Lateral strength variations and inelastic yielding in continental lithosphere, *Basin Res.,* **4,** 179–195.